An atmospheric chemist in search of the tropopause

Michael J. Prather,[1] Xin Zhu,[1] Qi Tang,[1] Juno Hsu,[1] and Jessica L. Neu[1,2]

Received 22 August 2010; revised 9 December 2010; accepted 29 December 2010; published 22 February 2011.

[1] Delineating the boundary between troposphere and stratosphere in a chemistry transport model requires a state variable for each air mass that maps out the ever shifting, overlapping three-dimensional (3-D) boundary at each time step. Using an artificial tracer, e90, with surface sources and 90 day decay time, the model e90 tropopause matches the 1-D temperature lapse rate definition of the tropopause as well as the seasonal variation of ozone at this boundary. This approach works from equator to pole, over all seasons, unlike methods based on potential vorticity or ozone. By focusing on the time scales that separate stratosphere from troposphere, we examine the cause of ozone seasonality at the midlatitude tropopause, the oldest air in the troposphere (winter descent in the subtropics), and a north-south bias in the age of air of the lowermost stratosphere as evaluated using a northern tracer. The tracer e90 is invaluable in 3-D modeling, readily separating stratosphere from troposphere and a giving quantitative measure of the effective distance from the tropopause.

Citation: Prather, M. J., X. Zhu, Q. Tang, J. Hsu, and J. L. Neu (2011), An atmospheric chemist in search of the tropopause, *J. Geophys. Res.*, *116*, D04306, doi:10.1029/2010JD014939.

1. Introduction

[2] To those interested in atmospheric composition and chemistry, the tropopause is a somewhat fuzzy, porous boundary between two chemically distinct regions: the stratosphere and the troposphere. The stratosphere has high ozone levels and short-wave ultraviolet photochemistry that destroys refractory greenhouse gases like nitrous oxide and chlorofluorocarbons; whereas the troposphere has precipitation and hydroxyl chemistry that rids the atmosphere of pollution and gases like methane. Being able to distinguish these two regions when modeling the atmosphere becomes important in both calculating chemistry and diagnosing processes that control atmospheric composition. In working with the University of California, Irvine (UCI), chemistry transport model (CTM), we have tried and found unworkable the traditional definitions of the tropopause because in complex situations they do not allow clear characterization of air masses as stratospheric versus tropospheric. We define here an approach that differentiates tropospheric air by time scales, linking it to the mixing of the troposphere and its exchange with the surface. This new definition of the tropopause is flexible and three-dimensional, and it is remarkably successful in matching the traditional diagnostics. This new diagnostic also helps us diagnose the large seasonal variation of ozone (O_3) at the midlatitude tropopause. By defining the aging of air since recent surface contact, we also identify old, photochemically aged air in the troposphere.

[3] A clear distinction between stratospheric vs. tropospheric air in three dimensions is necessary to diagnose chemical and dynamical budgets of trace gases, for example, the stratosphere-troposphere exchange (STE) of O_3 [*Holton et al.*, 1995; *Pierce et al.*, 2003; *Büker et al.*, 2005]. We wish to differentiate stratospheric from tropospheric air about the jet streams where there are often multiple tropopauses [*Randel et al.*, 2007]. We need to follow stratospheric intrusions as well as detached air masses within the troposphere [*Terao et al.*, 2008; *Pan et al.*, 2010] and down to the surface [*Lam and Fu*, 2010]. We must also recognize that there are regions where this boundary is fuzzy and at times ambiguous [*Tilmes et al.*, 2010]. Time scales for transport through the extratropical tropopause region have been studied with Lagrangian trajectories [*Berthet et al.*, 2007; *Hoor et al.*, 2010], but we seek an Eulerian approach.

[4] The traditional meteorological definition of the tropopause is based on the vertical static stability (also known as lapse rate): the lowest level at which the (negative) vertical gradient in temperature decreases to 2°C per km or less [*World Meteorological Organization* (*WMO*), 1995]. This WMO definition recognizes stratosphere-troposphere folds by allowing for a second tropopause above the first, but it does not identify the amount of tropospheric air between the two. With stratospheric folds, the lapse-rate tropopause identifies where the stratospheric air begins in an ascending profile, including the second tropopause, but not the transitions to tropospheric air. Alternatively, a stratospheric tracer, the potential vorticity (PV), can be used to define the tropopause [*Holton et al.*, 1995]. Since PV is ill defined at the equator, it cannot be used in the tropics, and the delineation of the tropopause shifts to potential temperature. Another stratospheric tracer, the O_3 abundance, is also used with some success to define the tropopause [*Hsu et al.*,

[1]Earth System Science Department, University of California, Irvine, California, USA.
[2]Now at Earth Atmospheric Science Division, Jet Propulsion Laboratory, Pasadena, California, USA.

0148-0227/11/2010JD014939

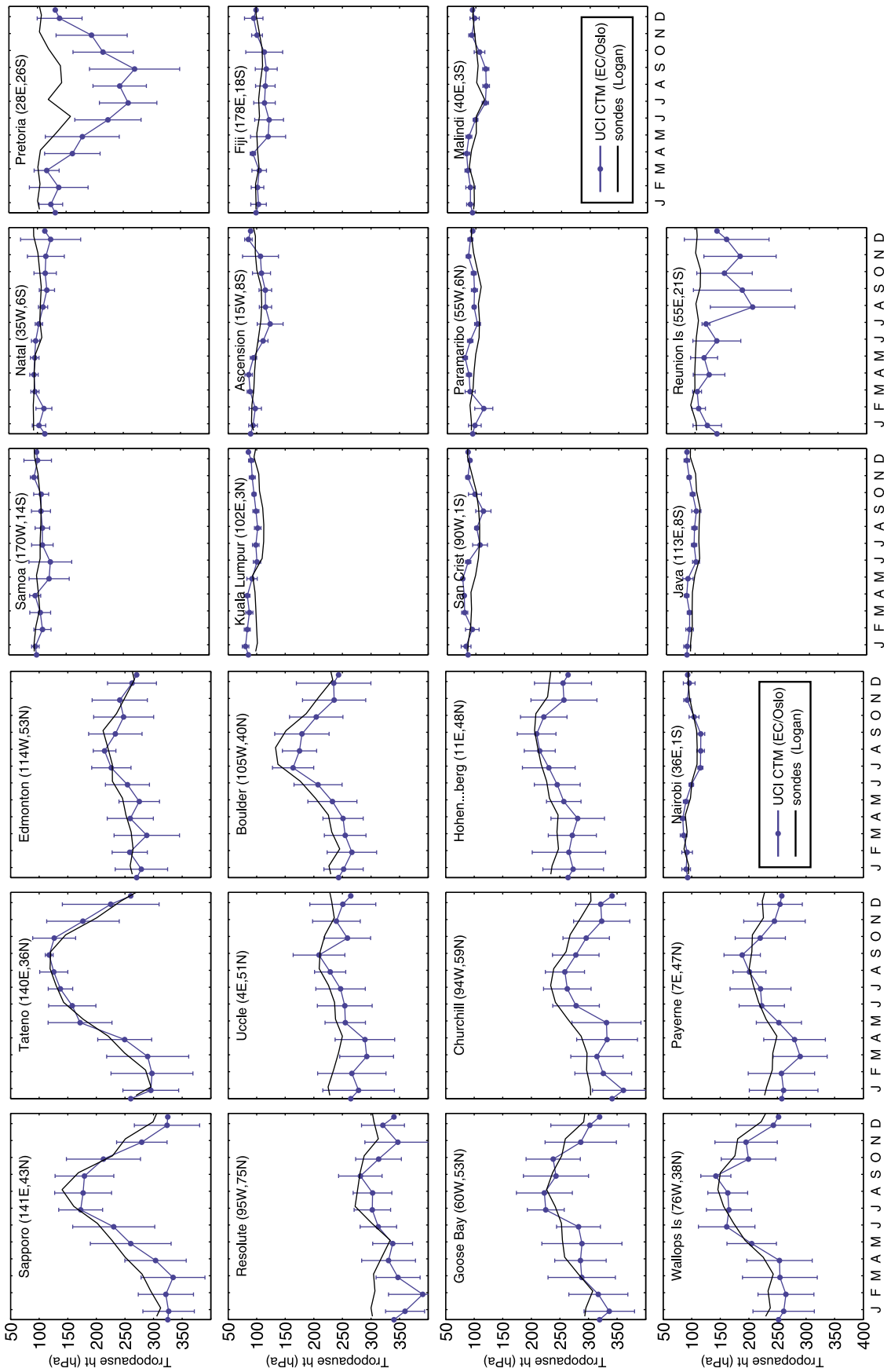
Sapporo (141E,43N)
Tateno (140E,36N)
Edmonton (114W,53N)
Samoa (170W,14S)
Natal (35W,6S)
Pretoria (28E,26S)
Resolute (95W,75N)
Uccle (4E,51N)
Boulder (105W,40N)
Kuala Lumpur (102E,3N)
Ascension (15W,8S)
Fiji (178E,18S)
Goose Bay (60W,53N)
Churchill (94W,59N)
Hohen...berg (11E,48N)
San Cristobal (90W,1S)
Paramaribo (55W,6N)
Malindi (40E,3S)
Wallops Is (76W,38N)
Payerne (7E,47N)
Nairobi (36E,1S)
Java (113E,8S)
Reunion Is (55E,21S)
UCI CTM (EC/Oslo)
sondes (Logan)
Tropopause ht (hPa)
J F M A M J J A S O N D

Figure 1

2005; *Wild*, 2007], but both O_3 and PV vary with latitude and season at the tropopause, and the criteria must be revised seasonally [*Logan*, 1999b, 1999a]. Other promising approaches involve static stability [*Homeyer et al.*, 2010]. We decided that a trace species with a time scale similar to the turnover of the troposphere would be optimal in defining the tropopause and, thus, experimented with artificial tracers emitted uniformly over the entire surface of the globe with e-fold decays of 30, 60, 90 and 180 days. We find that the 90 day e-fold tracer, e90, is optimal in mapping out the tropopause and stratosphere-troposphere folding events from equator to pole.

2. The e90 Tropopause and Ozone

[5] The e90 tracer has arbitrary scaling, and we choose emissions and molecular weight to give a global mean steady state abundance of 100 ppb, with values typically >125 ppb in the lower troposphere, and <50 ppb in most of the stratosphere. The tropopause value of e90 is derived from the single constraint that the troposphere annually comprises about 80% of the atmosphere (based on analysis of an early tropospheric O_3 climatology using O_3 = 100 ppb as the tropopause [*Prather et al.*, 2001]). For the current CTM and meteorology [*Hoor et al.*, 2009; *Hsu and Prather*, 2009], the e90 tropopause value is 90 ppb, and the monthly tropospheric fraction falls within the range 80.6 ± 0.5%. The tropopause boundary is fairly sharp; a change of ±2 ppb in e90 corresponds to only ±½% in air mass, or about 140 m altitude at the midlatitude tropopause.

[6] In these model calculations the UCI CTM is driven by meteorological fields derived from the European Centre for Medium-Range Weather Forecasts (ECMWF) Integrated Forecast System (IFS). For our model year 2004, the IFS cycle 31 is run at T159L60 to generate pieced forecasts (12 h spin-up, 24 h forecast). These forecasts are stored as 3 h averages, usually at lower resolution for CTM use. This unique approach for generating CTM meteorological fields was developed by the University of Oslo [*Kraabøl et al.*, 2002; *Isaksen et al.*, 2005]. Here our CTM uses these meteorological fields at a reduced T42L57 resolution (i.e., a 128 (longitude) by 64 (latitude) by 57 (altitude) grid). The horizontal resolution is a Gauss grid (N32, ~2.8°) and the L57 vertical layers are 0.5 km thick at 500 hPa, 0.8 km at 200 hPa, 1.0 km at 100 hPa, and 1.2 km at 50 hPa. With this vertical resolution at the tropopause and the numerical methods for tracer transport in the CTM [*Prather et al.*, 2008], we are able to simulate and resolve tropopause folds typically found in ozone sonde data [*Tang and Prather*, 2010].

[7] The monthly mean e90-tropopause pressures in the CTM are compared with the WMO lapse-rate definition from sondes in Figure 1. The tropopause pressures from many years of sondes at 23 sites are shown as a single mean value (black line) from the analysis of J. A. Logan and I. A. Megretskaia [*Logan*, 1999a, 1999b; *Considine et al.*, 2008]. The monthly mean and daily standard deviation from the model year 2004 are plotted as a blue line with dots and whiskers. Agreement in a climatological sense is excellent except in austral winter for the subtropical sites (Pretoria, Reunion I.), where multiple tropopauses with pressures ranging from 200 to 100 hPa are frequent [*Randel et al.*, 2007]. The sonde analysis always finds the uppermost, tropical tropopause about 100 hPa whereas the model more often finds the lower tropopause about 200–250 hPa, typical of midlatitudes. In this complex region the model error could be due to failure to vertically resolve the layer of tropospheric air above the jet using e90, to 2004 being an anomalous year, or to systematic errors in the ECMWF forecast fields near the southern subtropical jet. Analysis using coincident sondes profiles with multiple years might help resolve this.

[8] The tropopause O_3 observations are not readily simulated by models [*Considine et al.*, 2008]. Using e90 and our current CTM [*Hsu and Prather*, 2010; *Tang and Prather*, 2010] the modeled tropopause O_3 accurately reproduces the observations at least at northern midlatitudes as shown in Figure 2. The CTM's e90-tropopause O_3 (blue dots, line and whiskers) is shown with daily standard deviation for each month of year 2004 and the sonde monthly mean and standard deviations are for multiple years (black lines and whiskers [see *Logan*, 1999a, 1999b]). At some tropical sites the model reasonably matches the observations (Ascension, Fiji, Malindi, Natal, Paramaribo, Samoa), but at others the observations show year-round tropopause O_3 abundances to be well below 100 ppb, while the model is consistently above (Java, Kuala Lumpur, Nairobi, San Crist). This failing is seen in previous models [*Considine et al.*, 2008]. Since the tropopause heights are reasonable, the error is likely in the modeling of O_3 in this tropical tropopause transition region [*Fueglistaler et al.*, 2009]. Modeled O_3 abundances for the two southern subtropical sites (Pretoria, Reunion I.) are well below those observed, consistent with the lower altitude of the e90 tropopause.

[9] The Logan and Megretskaia analysis used here did not include any southern midlatitude stations. Our CTM predicts that O_3 abundances at the e90 tropopause are notably (30–40%) smaller than at equivalent latitudes in the northern midlatitudes (see later discussion of Figures 4 and 6). The recent climatology of O_3 profiles [*McPeters et al.*, 2007, Figure 4] shows averaged results at fixed pressure levels and not specifically the tropopause abundance. Nevertheless, the systematic north-south difference is clear: at 40°–50° latitude for pressure altitudes of 10 to 15 km, which spans the tropopause, the ratio of annual average SH O_3 abundances to NH abundances is about 0.75. In addition, we analyzed tropopause O_3 from 51 sondes for year 2004 from Lauder NZ (45°S, 170°E) obtained from the WOUDC in Canada: simple winter and summer averages give mean and standard deviation of tropopause O_3 abundances equal to 72 ± 21 and 117 ± 34 ppb, respectively, reproducing the

Figure 1. Monthly mean tropopause height (hPa) at 23 sonde sites. Observations (black line) are based on multiple years and supplied by J. A. Logan and I. A. Megretskaia [*Logan*, 1999b, 1999a]. UCI CTM modeled data (blue line with dots and whiskers) are from the e90 simulations using the EC/Oslo meteorological fields at T42L60 resolution for year 2004. Standard deviations of the daily modeled tropopause height (blue whiskers) are also shown.

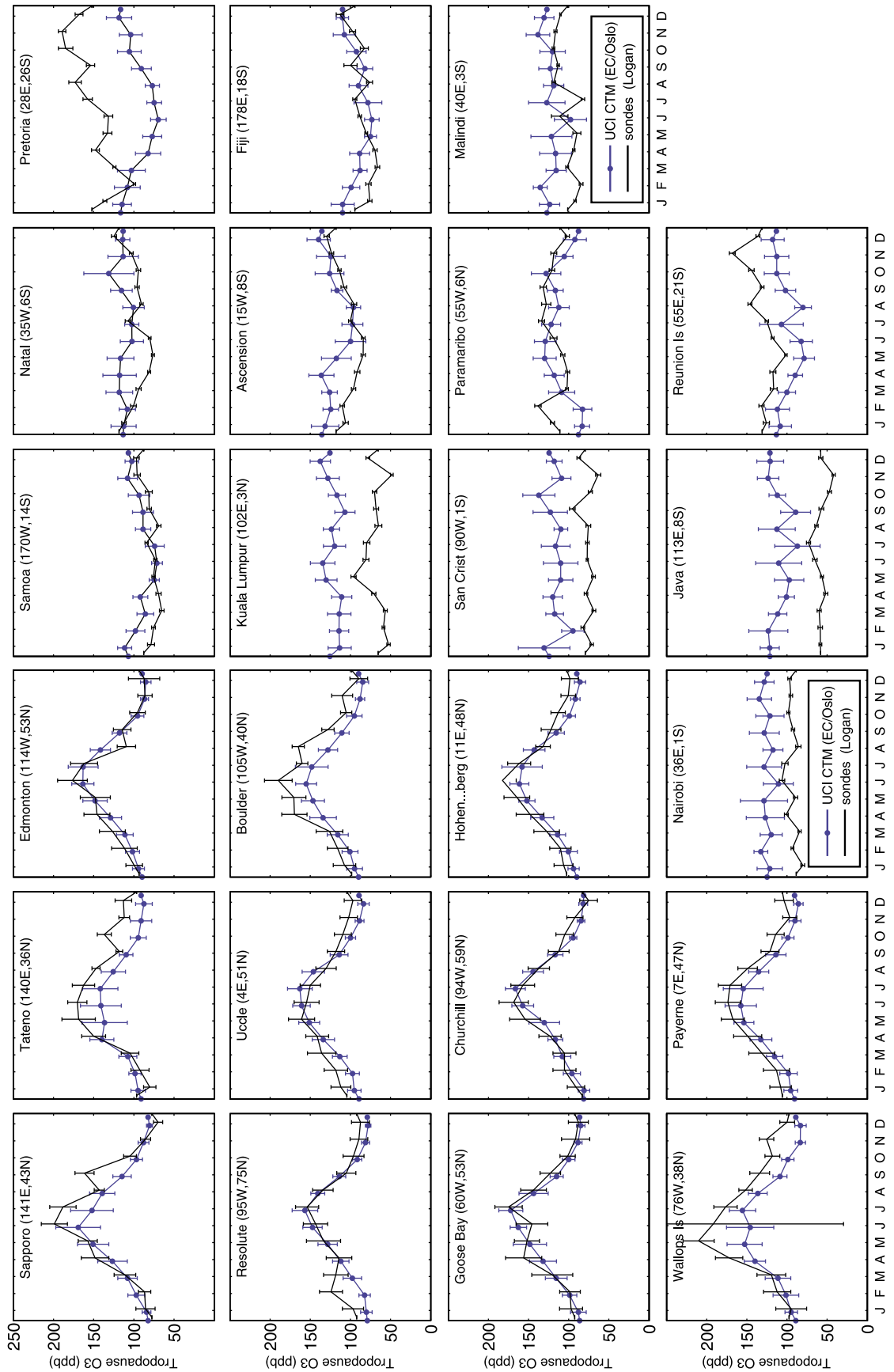

Figure 2. Monthly mean O_3 abundance (ppb) at the tropopause for the 23 sonde sites. See Figure 1. Both observations (black) and model (blue) shown with standard deviations as whiskers.

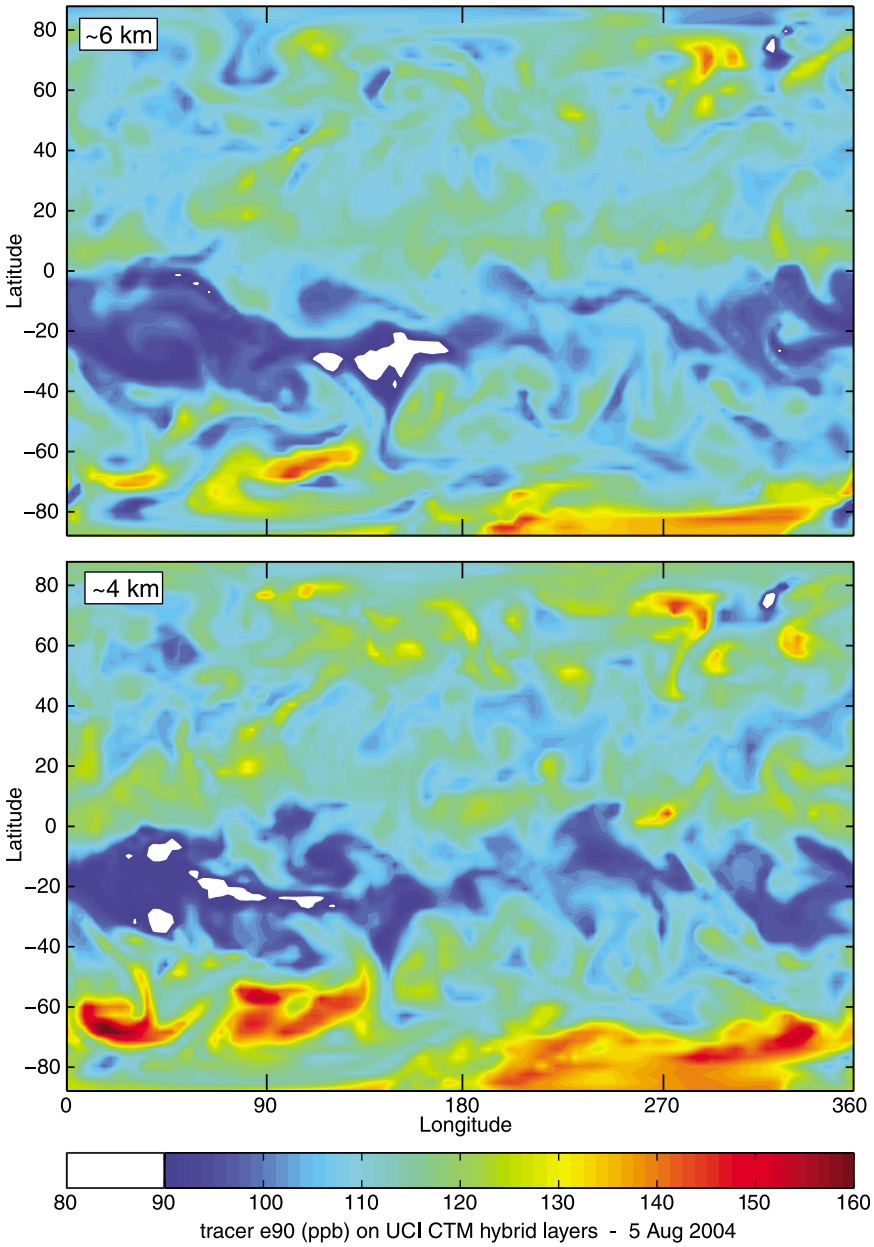

Figure 3. Global contours of e90 (ppb) on a latitude by longitude grid for CTM hybrid levels corresponding to (top) ~6 km and (bottom) ~4 km altitude on model date 5 August 2004, 0000 UT. Air masses with e90 < 90 ppb, nominally defining stratospheric air, are shown in white. The white areas in the southern subtropics have O_3 abundances about 50 to 70 ppb (not shown) indicating tropospheric origins, but the white area at 75°N has O_3 > 120 ppb and is clearly a stratospheric intrusion.

same seasonality as at 45°N but with about 30 ppb less O_3 than comparable northern latitudes, giving a SH:NH ratio about 0.7. Our CTM results give a somewhat smaller SH:NH ratio at 40°–50° of about 0.6 (see Figure 6 and later discussion on stratospheric age of air).

3. Oldest Air in the Troposphere

[10] Within the troposphere, the tracer e90 gives us information on the time since contact with the surface. Looking for the oldest air within the troposphere, we located the smallest e90 values in the wintertime subtropics in the lower troposphere. A snapshot of the latitude-by-longitude distribution of e90 on 5 August 2004 (0000 UT) is shown in Figure 3 for two model hybrid layers corresponding approximately to 4 and 6 km altitude. The white areas identify air with e90 < 90 ppb, ostensibly stratospheric. In the southern hemisphere (5°S to 35°S) this air is distinctly not stratospheric: the O_3 abundances are less than 70 ppb, and the e90 increases in air masses immediately above, indicating a more tropospheric origin. In contrast the small white area near 75°N at 4km has O_3 abundances >120 ppb and is connected directly with similar air mass above, typical of stratospheric intrusions. In our search for these

inadvertent e90 tropopauses (i.e., e90 < 90 ppb but O_3 < 80 ppb), we find them only in the descending branch of the Hadley cell of both hemispheres in wintertime, identifying the oldest tropospheric air, defined in terms of contact with the surface. During summer, there is sufficient deep convection to keep this descending air refreshed, but during winter, a small fraction can remain isolated and age until it comes in contact with the marine cumulus below 3 km altitude.

[11] Meridional transects at 112°W of O_3 and e90 are shown in Figure 4 for the same time as the latitude-by-longitude maps of e90 in Figure 3. At this longitude the oldest tropospheric air (e90 ~ 92 ppb) is seen at 15°S, 2–4 km altitude. Around the tropopause, white contours (e90 = 90 ppb) identify a complex fold region about 20°S. The patch of isolated tropospheric air about 14 km altitude connects to the troposphere about 102°W. At 45°N, a large stratospheric fold about the jet with O_3 > 300 ppb lies underneath air with O_3 < 200 ppb, where the latter air is close to tropospheric as identified by e90. Also apparent in Figure 4, the O_3 abundances at the e90 tropopause are notably larger in the north than in the south, as corroborated by the observations discussed above. The differences shown in Figure 4 for August are exaggerated, however, contrasting boreal summer (max) versus austral winter (min). All of these O_3 features are clearly seen in the e90 contours and would not be readily identified using a lapse-rate tropopause. In addition, this e90 diagnostic works across all latitudes and seasons.

[12] The frequency and chemical characteristics of the oldest tropospheric air are examined for Mauna Loa, Hawaii with the hope of identifying chemical signatures that might be observed. Figure 5 shows the O_3 versus e90 scatter plot of Mauna Loa sampling for January–February and July–August 2004. In summer, as expected, all air masses have e90 > 100 ppb; but in winter, air with e90 < 95 ppb is seen about 2% of the time. This air is clearly tropospheric and is unique in having a very small range in O_3 abundances, 51–55 ppb as compared with the overall range of 20–85 ppb. A unique chemical property of this oldest air near Mauna Loa in winter is its uniform character: CO, 58–62 ppb; C_2H_6, 300–350 ppt; H_2O_2, 0.6–0.7 ppb; NO_x, 17–20 ppt (not shown). If there were a clear way to identify this air, then Mauna Loa measurements could provide an observational test of the photochemical aging of tropical air.

4. Cause of Tropopause O_3 Seasonality

[13] The seasonal cycle of tropopause O_3 at northern midlatitudes is large, with winter-to-summer monthly means ranging typically from 90 to 160 ppb (Figure 2). A comparison of zonal averages at 40°N and 40°S (Figure 6) shows the much smaller seasonal amplitude and absolute values in the southern hemisphere, in general agreement with observations noted earlier. Both seasonal cycles show an early summer maximum (1 January to 1 February at 40°S, 1 June to 1 July at 40°N). The seasonality of O_3 in the lower stratosphere about 400 m above the tropopause (e90 = 84 ppb, Figure 6) parallels the tropopause values, and abundances are uniformly 15% (40°N) to 20% (40°S) greater [see *Logan*, 1999b, Figure 10].

[14] The O_3 increase from winter to summer could be caused by either chemistry (i.e., an increase in net production of O_3 during summer) or dynamics (i.e., movement of air with higher O_3 abundances from about 1 km above the tropopause down to the tropopause, with the consequent removal of the air below by STE). The dynamical descent hypothesis would predict that the higher summertime tropopause O_3 would be accompanied by greater stratospheric age of air.

[15] Age of air (AoA) is defined as the mean age of a stratospheric air mass since the air comprising that mass entered the stratosphere [*Neu and Plumb*, 1999; *Hall and Waugh*, 2000]. In practice this formal definition is not easy to evaluate with high precision in either models or measurements as the calculation is obfuscated by air entering the stratosphere at a range of locations with a range of trace gas abundances. The observed AoA uses long-lived, quasi-inert trace gases in the stratosphere that have almost linearly increasing tropospheric abundances over the previous decade. The two primary gases are CO_2 and SF_6 [e.g., *Boering et al.*, 1996; *Engel et al.*, 2009], both of which are driven by northern midlatitude sources. Thus, there is a north-south gradient in these species across the tropics even at the tropopause, and a range in the average abundance of air entering the stratosphere. We use a traditional approach to model the AoA by calculating the steady state distribution of a conserved tracer with a constant fossil fuel CO_2 emission pattern [*Gurney et al.*, 2003; *Prather et al.*, 2008]. In practice we initiate the model with zero CO_2 and run for 20 years repeating the year 2004 meteorological fields. The instantaneous AoA is calculated by subtracting a reference zero-age value (meant to be the mean tropical tropopause abundance) and dividing by the annual growth rate of CO_2. To pick a single, nonseasonally varying, reference value for tropopause abundances, we average the block 20°S–20°N by 12–16 km over all longitudes. This zero-age definition is consistent, to within a constant offset, with the observational derivation of age of air using the approximately linearly increasing rate of either CO_2 or SF_6 [*Boering et al.*, 1996; *Bönisch et al.*, 2009; *Engel et al.*, 2009].

[16] The seasonal cycle of AoA in the lowermost stratosphere at midlatitudes is different in each hemisphere (Figure 6) and likely reflects their different wintertime circulations. The 40°N cycle peaks in late summer (1 August) with a range of 0.2 years, and the 40°S cycle peaks near the summer equinox (1 January) with a range of 0.1 year.

[17] Given that AoA at 40°N is larger in summer than winter by +0.20 years, one can use the observed trace gas correlations to estimate the corresponding increase in O_3. Trace gases in the lower, extratropical stratosphere are observed to be tightly correlated with a slope equal to the ratio of their fluxes coming into or out of the stratosphere, as proposed by theory [*Plumb and Ko*, 1992] and verified in 3-D CTMs [*Avallone and Prather*, 1997; *Olsen et al.*, 2001]. Trace gas correlations in the NH midlatitude stratosphere are well established by observations, and we can use published data to derive an empirical ratio O_3:AoA = 280 ppb/yr. This relationship is calculated by combining four observed ratios: the growth rate SF_6:AoA = 0.23 ppt/yr [*Levin et al.*, 2010] plus the observed ratios of SF_6:N_2O = 0.0212 ppt/ppb [*Bönisch et al.*, 2009, Figure 1]; NO_y:N_2O = −0.085 [*Olsen et al.*, 2001]; NO_y:O_3 = 0.0033 [*Murphy and Fahey*, 1994; *Olsen et al.*, 2001]. In our model, from 20°N to 90°N, a similar but slightly smaller value of O_3:

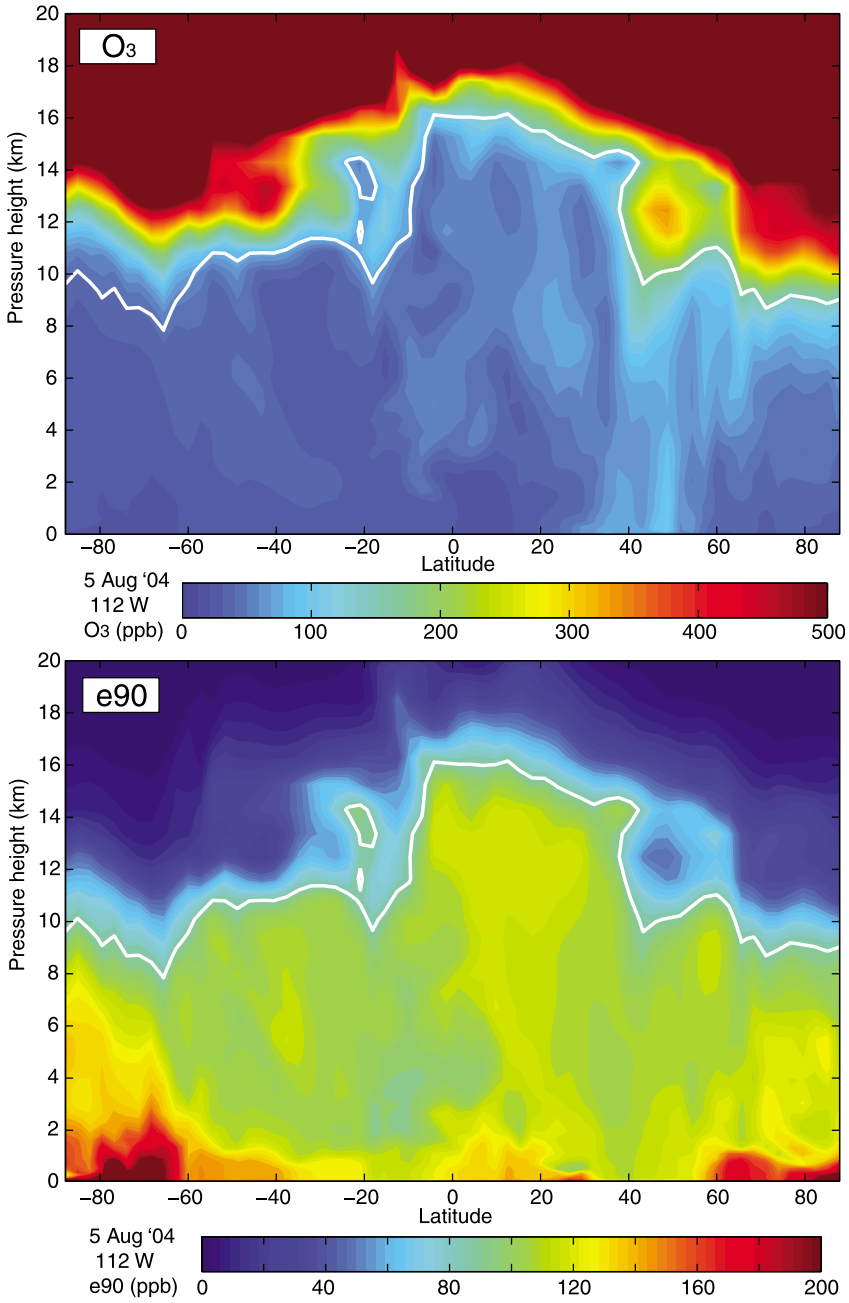

Figure 4. Meridional transects (latitude by height) at 112°W longitude on 5 August 2004, 0000 UT of (top) O_3 and (bottom) e90. Color mapping of O_3 accentuates the troposphere and lower stratosphere (0–500 ppb), while that of e90 covers its full range (0–200 ppb). The white contour in both panels is the 90 ppb level of e90, corresponding to the tropopause. The isolated contour of tropospheric air above the southern jet at about 20°S indicates a double tropopause and complex fold that connects to the troposphere at 102°W (not shown) where an isolated stratospheric air mass appears below the second tropopause.

AoA = 200 ± 50(s.d.) ppb/yr can be calculated from the relative differences between e90 values of 90 and 84 ppb (40°N shown in Figures 6a and 6b). Although the O_3 increase 400 m above the tropopause is similar at 40°N and 40°S (Figure 6a), the increase in AoA above the tropopause is much less at 40°S than at 40°N (Figure 6b) because it is defined with a northern source. Thus the southern midlatitude value of O_3:AoA is much larger, 700 ± 150 ppb/yr.

[18] The peak-to-peak range of tropopause O_3 at 40°N–50°N ranges from 75 to 90 ppb, and the corresponding AoA range is about 0.19 ± 0.02 years. Thus, a little over half, at most about 50 ppb, of the O_3 increase could possibly be associated directly with this change in AoA. Moreover, the seasonal cycles of O_3 and AoA are out of phase, with AoA at 40°N peaking later, at the end of summer. A scatter plot of tropopause O_3 versus AoA at 40°N (pointed out by a

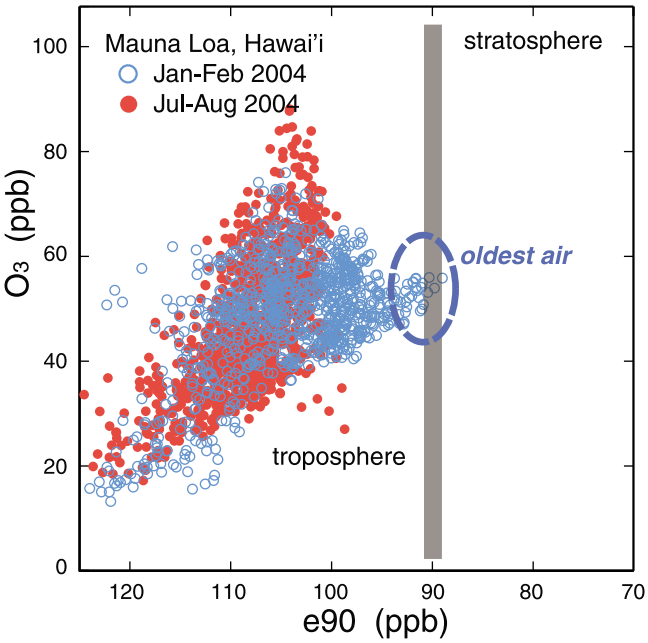

Figure 5. Scatterplot of O_3 (ppb) vs. e90 (ppb) from the UCI CTM sampled at the location of Mauna Loa, Hawaii and at altitudes 3–4 km. Two summer months (July–August, solid red circles) and two winter months (January–February, open blue circles) are shown. The nominal tropopause e90 values are marked with a vertical gray bar, and stratospheric air here has $O_3 > 100$ ppb. The oldest tropospheric air masses (winter only) are highlighted by the dashed blue oval. Each period includes about 960 samples.

reviewer, but not shown here) produces a broad circle of monthly points with no clear slope associated with descent (i.e., 200 ppb/yr). A similar plot at 40°S has a more compact relationship but with a much smaller slope than expected for southern midlatitudes. We conclude that some, but probably less than half, of the January-to-July increase in O_3 at the northern midlatitude tropopause can be simply accounted for by descent of older, high-O_3 stratospheric air.

[19] A fraction of the summertime increase can also be due to photochemistry. The net production or loss of O_3 in the extratropical lower stratosphere (outside the Antarctic ozone hole) is slow, for example, in the region 40°N–60°N latitude at 360–380 K potential temperature, production is less than 10 ppb per month in peak summer. In the subtropics, however, net production of O_3 by photolysis of O_2 occurs throughout the lower stratosphere and even into the upper troposphere [*Prather*, 2009]. Photolysis follows the Sun and peaks at 25°N in June, producing as much as 30–60 ppb per month at 380–400 K, and this source can contribute to the summertime increase at midlatitudes through mixing along isentropes. The O_3 summer maximum continues well into the lower stratosphere, at least to the 500 ppb level, and is consistent with a combination of dynamical and chemical causes.

[20] The early summer maximum in tropopause O_3 is paralleled in the upper troposphere, although with a much smaller peak-to-peak range of 30 ppb [*Logan*, 1999b]. While the latter obviously cannot force the observed amplitude of the former, both may be driven in part by the same mechanism, perhaps enhanced STE. Tropospheric seasonality alters the effective lower boundary of stratospheric O_3 and the 30 ppb cycle may propagate into the lowermost stratosphere. It is likely that all three factors–stratospheric dynamics, stratospheric chemistry, and tropospheric abundances–contribute to the seasonal cycle of lower stratospheric O_3 in the northern hemisphere, but in the southern hemisphere, dynamics and descent may explain most of the seasonality.

5. Age-of-Air Bias in the Lowermost Stratosphere

[21] Comparing the AoA at the e90 tropopause (Figure 6), we find a clear difference between northern (−0.45 years) and southern (+0.35 years) midlatitudes. This difference of

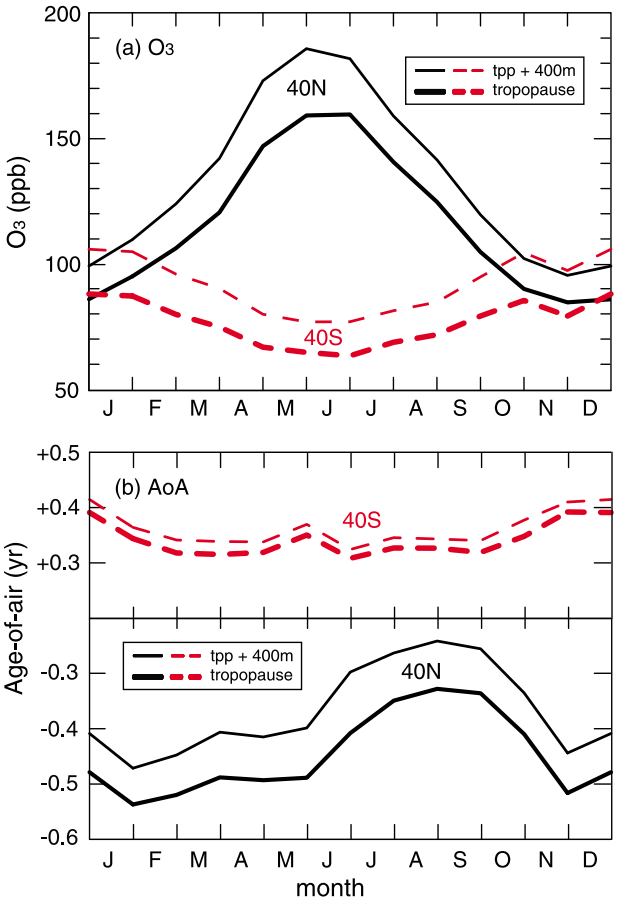

Figure 6. Annual cycle of (a) O_3 (ppb) and (b) age of air (years) in the lowermost stratosphere. Values are shown for the first of each month in year 2004 for 40°N (±4°) (black solid lines) and 40°S (±4°) (red dashed lines) averaged over all longitudes. Tropopause values (e90 = 90 ppb) are denoted by thick lines; and the e90 level of 84 ppb (about 400 m above the tropopause) is denoted by thin lines. Age of air is calculated with a fossil fuel emission pattern of CO_2. Calculation of O_3 and age of air at e90 values of 90 and 84 ppb is based on interpolation of individual, instantaneous model profiles. If an averaging procedure is used (i.e., all model layers with e90 between 88 and 92 ppb), then the tropopause O_3 values are overestimated by a factor of 1.7 because of the asymmetric shape of the profile.

0.8 years continues into the lowermost stratosphere, reducing to 0.7 years at 400 m above the tropopause (Figure 6b), about 0.3 years at O_3 abundances of 400 ppb, and 0.1 years or less at 1000 ppb (not shown). This apparent hemispheric bias in the AoA is due to the method of both observing and modeling age of air; that is, we force the annual increase in troposphere CO_2 with northern midlatitude sources and hence there is a north-south gradient at the tropical tropopause. In our model, tropospheric air does not enter the stratosphere at a single fixed point all year. More air enters the southern midlatitude lower stratosphere from the southern tropics or jet region with lower CO_2 abundance than equivalent northern air, and hence appears older. Indeed, if we repeat our AoA calculations with the CO_2 emitted from a tropical band (20°S–20°N), the north-south differences disappear, with both 40°S and 40°N having an average AoA of about +0.3 years at the tropopause. Since the observational analysis of AoA typically uses CO_2 or SF_6, whose increases are also driven by northern sources [*Levin et al.*, 2010], the comparison between model and measurements remains valid.

[22] We find no clear data to test the north-south asymmetry of AoA simulated in our model. For example, AoA measurements [e.g., *Waugh and Hall*, 2002, Figure 6] do not provide enough consistent measurements at the tropopause level in both hemispheres. The best latitudinal data are from the ER-2 data (20 km, O_3 > 800 ppb), where we calculate the AoA becomes similar in both hemispheres. Most of the detailed correlations that might clearly identify this bias, such as the SF_6-N_2O correlations about the tropopause, are only from the northern hemisphere [*Bönisch et al.*, 2009, Figure 1]. The new pole-to-pole latitudinal transects by the HIAPER (High-performance Instrumented Airborne Platform) Pole-to-Pole Observations (HIPPO) should resolve this [see *Pan et al.*, 2010]. We predict that these observations should show a much flatter SF_6:N_2O slope for N_2O abundances between 320 and 300 ppb, consistent with the small vertical gradient of AoA across the tropopause in southern midlatitudes. One possibility remains that the ECMWF meteorological data are in error and accentuate the north-south gradient of air entering the stratosphere.

6. Discussion

[23] The use of a short-lived, surface-emitted tracer like e90 in atmospheric chemistry models provides unique and valuable information for diagnosing the chemistry of the troposphere and lower stratosphere. It quantifies the rate of mixing of tropospheric air and defines the tropopause. For air in the lower stratosphere, it gives a measure of distance from the tropopause as measured by the amount of recently incorporated tropospheric air. For the most part, e90 provides accurate, three-dimensional, year-round discrimination of the stratosphere-troposphere boundary. Using our CTM with ECMWF forecast meteorological fields, we can reproduce, for the most part, the observed absolute abundance and seasonal cycle of O_3 at the tropopause in midlatitudes. Diagnosis of the seasonal cycles of both O_3 and AoA allows us to track the causes of such seasonality.

[24] Some clear discrepancies in our CTM remain in the subtropics and tropics. In the southern subtropics the model diagnoses a second tropopause but underestimates the occurrence of the upper one. The errors could be in the meteorological data or in the numerical methods. At some of the tropical sites we predict much larger tropopause O_3 abundances than observed, and this is associated with a transition layer below the tropopause with elevated O_3, which is not seen in the sondes.

[25] With the e90 tracer, we have identified the oldest air in the troposphere, which is surprisingly homogeneous. If observable it may provide a test of the long-term photochemical evolution of semi-isolated tropospheric air masses, and O_3 in particular.

[26] The tropopause defined with e90 requires calculation of a tracer consistent with the meteorological data. This methodology is unsatisfying for those wishing to define the tropopause merely from the meteorological data, yet it would seem logical that we also investigate the tropopause region from a tropospheric point of view, using something like e90. Using stratospheric quantities like O_3 or PV to define the tropopause obviously includes the effects of convection and other mixing, but the seasonal variations in these quantities, or the problems in the tropics, makes for a more difficult, possibly subjective, determination of the stratosphere-troposphere boundary, particularly in regions of folds about the jet stream.

[27] **Acknowledgments.** We are indebted to the indefatigable reviewers for their insightful and constructive suggestions that have clarified our results and greatly improved the paper. This research has been supported at UC Irvine by the National Aeronautics and Space Administration (grants NNG06GB84G and NNX08AR25G), the National Science Foundation (NSF ATM-0550234), and the Kavli Foundation.

References

Avallone, L. M., and M. J. Prather (1997), Tracer-tracer correlations: Three-dimensional model simulations and comparisons to observations, *J. Geophys. Res.*, *102*(D15), 19,233–19,246, doi:10.1029/97JD01123.

Berthet, G., J. G. Esler, and P. H. Haynes (2007), A Lagrangian perspective of the tropopause and the ventilation of the lowermost stratosphere, *J. Geophys. Res.*, *112*, D18102, doi:10.1029/2006JD008295.

Boering, K. A., S. C. Wofsy, B. C. Daube, H. R. Schneider, M. Loewenstein, and J. R. Podolske (1996), Stratospheric mean ages and transport rates from observations of carbon dioxide and nitrous oxide, *Science*, *274*(5291), 1340–1343, doi:10.1126/science.274.5291.1340.

Bönisch, H., A. Engel, J. Curtius, T. Birner, and P. Hoor (2009), Quantifying transport into the lowermost stratosphere using simultaneous in-situ measurements of SF_6 and CO_2, *Atmos. Chem. Phys.*, *9*(16), 5905–5919, doi:10.5194/acp-9-5905-2009.

Büker, M. L., M. H. Hitchman, G. J. Tripoli, R. B. Pierce, E. V. Browell, and M. A. Avery (2005), Resolution dependence of cross-tropopause ozone transport over east Asia, *J. Geophys. Res.*, *110*, D03107, doi:10.1029/2004JD004739.

Considine, D. B., J. A. Logan, and M. A. Olsen (2008), Evaluation of near-tropopause ozone distributions in the Global Modeling Initiative combined stratosphere/troposphere model with ozonesonde data, *Atmos. Chem. Phys.*, *8*(9), 2365–2385, doi:10.5194/acp-8-2365-2008.

Engel, A., et al. (2009), Age of stratospheric air unchanged within uncertainties over the past 30 years, *Nat. Geosci.*, *2*(1), 28–31, doi:10.1038/ngeo388.

Fueglistaler, S., A. E. Dessler, T. J. Dunkerton, I. Folkins, Q. Fu, and P. W. Mote (2009), Tropical Tropopause Layer, *Rev. Geophys.*, *47*, RG1004, doi:10.1029/2008RG000267.

Gurney, K. R., et al. (2003), TransCom3 CO_2 inversion intercomparison: 1. Annual mean control results and sensitivity to transport and prior flux information, *Tellus, Ser. B*, *55*(2), 555–579, doi:10.1034/j.1600-0889.2003.00049.x.

Hall, T. M., and D. W. Waugh (2000), Stratospheric residence time and its relationship to mean age, *J. Geophys. Res.*, *105*(D5), 6773–6782, doi:10.1029/1999JD901096.

Holton, J. R., P. H. Haynes, M. E. Mcintyre, A. R. Douglass, R. B. Rood, and L. Pfister (1995), Stratosphere-troposphere exchange, *Rev. Geophys.*, *33*(4), 403–439, doi:10.1029/95RG02097.

Homeyer, C. R., K. P. Bowman, and L. L. Pan (2010), Extratropical tropopause transition layer characteristics from high-resolution sounding data, *J. Geophys. Res.*, *115*, D13108, doi:10.1029/2009JD013664.

Hoor, P., et al. (2009), The impact of traffic emissions on atmospheric ozone and OH: Results from QUANTIFY, *Atmos. Chem. Phys.*, *9*(9), 3113–3136, doi:10.5194/acp-9-3113-2009.

Hoor, P., H. Wernli, M. I. Hegglin, and H. Bönisch (2010), Transport timescales and tracer properties in the extratropical UTLS, *Atmos. Chem. Phys.*, *10*(16), 7929–7944, doi:10.5194/acp-10-7929-2010.

Hsu, J., and M. J. Prather (2009), Stratospheric variability and tropospheric ozone, *J. Geophys. Res.*, *114*, D06102, doi:10.1029/2008JD010942.

Hsu, J., and M. J. Prather (2010), Global long-lived chemical modes excited in a 3-D chemistry transport model: Stratospheric N_2O, NO_y, O_3 and CH_4 chemistry, *Geophys. Res. Lett.*, *37*, L07805, doi:10.1029/2009GL042243.

Hsu, J., M. J. Prather, and O. Wild (2005), Diagnosing the stratosphere-to-troposphere flux of ozone in a chemistry transport model, *J. Geophys. Res.*, *110*, D19305, doi:10.1029/2005JD006045.

Isaksen, I. S. A., C. Zerefos, K. Kourtidis, C. Meleti, S. B. Dalsoren, J. K. Sundet, A. Grini, P. Zanis, and D. Balis (2005), Tropospheric ozone changes at unpolluted and semipolluted regions induced by stratospheric ozone changes, *J. Geophys. Res.*, *110*, D02302, doi:10.1029/2004JD004618.

Kraabøl, A. G., T. K. Berntsen, J. K. Sundet, and F. Stordal (2002), Impacts of NO_x emissions from subsonic aircraft in a global three-dimensional chemistry transport model including plume processes, *J. Geophys. Res.*, *107*(D22), 4655, doi:10.1029/2001JD001019.

Lam, Y. F., and J. S. Fu (2010), A novel downscaling technique for the linkage of global and regional air quality modeling, *Atmos. Chem. Phys.*, *10*(8), 4013–4031, doi:10.5194/acp-10-4013-2010.

Levin, I., et al. (2010), The global SF_6 source inferred from long-term high precision atmospheric measurements and its comparison with emission inventories, *Atmos. Chem. Phys.*, *10*(6), 2655–2662, doi:10.5194/acp-10-2655-2010.

Logan, J. A. (1999a), An analysis of ozonesonde data for the lower stratosphere: Recommendations for testing models, *J. Geophys. Res.*, *104*(D13), 16,151–16,170, doi:10.1029/1999JD900216.

Logan, J. A. (1999b), An analysis of ozonesonde data for the troposphere: Recommendations for testing 3-D models and development of a gridded climatology for tropospheric ozone, *J. Geophys. Res.*, *104*(D13), 16,115–16,149, doi:10.1029/1998JD100096.

McPeters, R. D., G. J. Labow, and J. A. Logan (2007), Ozone climatological profiles for satellite retrieval algorithms, *J. Geophys. Res.*, *112*, D05308, doi:10.1029/2005JD006823.

Murphy, D. M., and D. W. Fahey (1994), An estimate of the flux of stratospheric reactive nitrogen and ozone into the troposphere, *J. Geophys. Res.*, *99*(D3), 5325–5332, doi:10.1029/93JD03558.

Neu, J. L., and R. A. Plumb (1999), Age of air in a "leaky pipe" model of stratospheric transport, *J. Geophys. Res.*, *104*(D16), 19,243–19,255, doi:10.1029/1999JD900251.

Olsen, S. C., C. A. McLinden, and M. J. Prather (2001), Stratospheric N_2O-NO_y system: Testing uncertainties in a three-dimensional framework, *J. Geophys. Res.*, *106*(D22), 28,771–28,784, doi:10.1029/2001JD000559.

Pan, L. L., et al. (2010), The Stratosphere-Troposphere Analyses of Regional Transport 2008 experiment, *Bull. Am. Meteorol. Soc.*, *91*(3), 327–342, doi:10.1175/2009BAMS2865.1.

Pierce, R. B., et al. (2003), Regional Air Quality Modeling System (RAQMS) predictions of the tropospheric ozone budget over East Asia, *J. Geophys. Res.*, *108*(D21), 8825, doi:10.1029/2002JD003176.

Plumb, R. A., and M. K. W. Ko (1992), Interrelationships between mixing ratios of long lived stratospheric constituents, *J. Geophys. Res.*, *97*(D9), 10,145–10,156.

Prather, M. J. (2009), Tropospheric O_3 from photolysis of O_2, *Geophys. Res. Lett.*, *36*, L03811, doi:10.1029/2008GL036851.

Prather, M., et al. (2001), Atmospheric chemistry and greenhouse gases, in *Climate Change 2001: The Scientific Basis. Third Assessment Report of the Intergovernmental Panel on Climate Change*, edited by J. T. Houghton et al., pp. 239–287, Cambridge Univ. Press, Cambridge, U. K.

Prather, M. J., X. Zhu, S. E. Strahan, S. D. Steenrod, and J. M. Rodriguez (2008), Quantifying errors in trace species transport modeling, *Proc. Natl. Acad. Sci. U. S. A.*, *105*(50), 19,617–19,621, doi:10.1073/pnas.0806541106.

Randel, W. J., D. J. Seidel, and L. L. Pan (2007), Observational characteristics of double tropopauses, *J. Geophys. Res.*, *112*, D07309, doi:10.1029/2006JD007904.

Tang, Q., and M. J. Prather (2010), Correlating tropospheric column ozone with tropopause folds: the Aura-OMI satellite data, *Atmos. Chem. Phys.*, *10*(19), 9681–9688, doi:10.5194/acp-10-9681-2010.

Terao, Y., J. A. Logan, A. R. Douglass, and R. S. Stolarski (2008), Contribution of stratospheric ozone to the interannual variability of tropospheric ozone in the northern extratropics, *J. Geophys. Res.*, *113*, D18309, doi:10.1029/2008JD009854.

Tilmes, S., et al. (2010), An aircraft-based upper troposphere lower stratosphere O_3, CO, and H_2O climatology for the Northern Hemisphere, *J. Geophys. Res.*, *115*, D14303, doi:10.1029/2009JD012731.

Waugh, D. W., and T. M. Hall (2002), Age of stratospheric air: Theory, observations, and models, *Rev. Geophys.*, *40*(4), 1010, doi:10.1029/2000RG000101.

Wild, O. (2007), Modelling the global tropospheric ozone budget: exploring the variability in current models, *Atmos. Chem. Phys.*, *7*(10), 2643–2660, doi:10.5194/acp-7-2643-2007.

World Meteorological Organization (WMO) (1995), Manual on codes: International codes, vol. I.1, part A, WMO–No. 306, Geneva. (Available at http://www.wmo.int/pages/prog/www/WMOCodes/Manual/WMO306_Vol-I-1-PartA.pdf)

J. Hsu, M. J. Prather, Q. Tang, and X. Zhu, Earth System Science Department, University of California, 3329 Croul Hall, Irvine, CA 92697-3100, USA. (mprather@uci.edu)

J. L. Neu, Earth Atmospheric Science Division, Jet Propulsion Laboratory, Pasadena, CA 91109, USA.